CHAPTER 1

4-D Seismic Monitoring of Reservoir Production in the Eugene Island 330 Field, Gulf of Mexico

Roger N. Anderson*, Albert Boulanger*, Wei He*, Y. F. Sun*, Liqing Xu*, and Bruce Hart**

Anderson, R. N., A. Boulanger, Wei He, Y. F. Sun, Liquing Xu, and B. Hart, 4-D seismic monitoring of reservoir production in the Eugene Island 330 Field, Gulf of Mexico, *in* P. Weimer and T. L. Davis, eds., *AAPG Studies in Geology No. 42* and *SEG Geophysical Developments Series No. 5*, AAPG/SEG, Tulsa, p. 9–20.

ABSTRACT

We have begun the integration of rock physical properties, production data, reservoir modeling, and 4-D seismic monitoring from multiple generations of 3-D surveys to track changes of seismic attributes with pool drainage. Here we present the 4-D seismic monitoring technologies in order to (1) predict reservoir characteristics from seismic data, (2) locate bypassed pay, and (3) isolate drilling strategies that will maximize additional recovery for future fields. The test study is from the Eugene Island 330 Field of the offshore Gulf of Mexico. These results will have general application to other fields in the Gulf of Mexico, Nigeria, the North Sea, the Caspian Sea, and Indonesia—those with multiple generations of 3-D seismic coverage and seismically illuminated hydrocarbons.

INTRODUCTION

3-D seismic technologies have progressed to the point that the data are being applied to reservoir production and engineering problems in addition to the original exploration uses. In addition, 4-D, or time-lapse, seismic monitoring is beginning to offer the possibility that control of field development may someday be possible through the merging of seismic reservoir simulations and field-monitored changes in impedance. Understanding the link between stratigraphy, fluid content, and changes in seismic response is a prerequisite to being able to confidently identify and quantify hydrocarbon drainage through the monitoring of 4-D seismic amplitude changes over time.

Changes in seismic amplitude within a given reservoir during its production history can be caused by changes in gas/oil/water ratios, in reservoir pressures, and/or in fluid contact levels, as well as by acquisition and geometry changes between surveys. We use wireline (sonic, density, porosity, water saturation [Sw] variations over time) and production (pressure, water cut, gas/oil ratio) data to produce forward models of acoustic impedance changes as reservoirs are produced. The model results allow us to predict the changes in seismic response that should be imaged by our 4-D seismic monitoring technologies. In order to extract the observed changes, we normalize different vintages of 3-D seismic surveys and examine resultant similarities and differences. The match between model and observed changes allows the prediction of location and composition of bypassed pay for future targeting.

*Lamont Doherty Earth Observatory, Columbia University, New York, NY 10964

**Pennsylvania State University, State College, Pennsylvania; now at New Mexico Bureau of Mines, Socorro, NM 87801

EUGENE ISLAND (EI) 330 FIELD

To develop these seismic monitoring technologies, we analyzed two fault blocks of the LF reservoir along the EI 330/338 block boundary in the EI 330 field of offshore Louisiana (Oil and Gas Journal), Nov. 4, 1991; April 26, 1993; June 6, 1994; March 28/April 4, 1995, and May 18, 1996) (Figure 1). This field has produced more than 500 MMBOE since 1972, with oil and gas produced from various stacked sand reservoirs (Figure 2) in rollover anticlines and fault blocks associated with large regional (the Red) and counter-regional (the Blue) growth faults and smaller antithetic faults (e.g., the F fault) (Figure 3) (cf. Holland et al., 1990; Alexander and Flemings, 1995). The ongoing development of this field and the remarkable amount of seismic, production, geochemical, and wireline data available from the field make this an ideal location to research the effects of production and fluid migration on changing acoustic (seismic) signals over time.

In the EI 330 field, we have access to three vintages of 3-D seismic surveys (1985, 1988, and 1992; Figure 1). These surveys include the 1992 Shell/Exxon survey centered on Block 331 (Sh) (reflection and acoustic impedance versions), as well as the Texaco/Chevron 1988 survey over Blocks 338 and 339 (Tx) and the Pennzoil/Mobil/BP 1985 survey centered on Block 330 (Pz). We also have compiled >550 wireline logs from the field and have access to the production data from more than 300 wells in the field. We have conducted stratigraphic studies on multiple scales throughout the field (cf. Alexander and Flemings, 1995, and Hart et al., 1995). Combined stratigraphic, structural, and seismic attribute analysis have shown how depositional features and faults can compartmentalize reservoirs in this field. Hart et al., this volume, for example, imaged clinoforms controlling drainage in the GA reservoir of blocks 338/339. We have deepened a well into the Red fault zone, thought to be the major conduit for hydrocarbon migration in the area, collected oils from the fault zone; cored the fractured, geopressured shales adjacent to the fault; and conducted in situ stress and permeability measurements in the fault zone (purple line in Figure 3; Anderson et al., 1995a, 1995b.) (A CD-ROM of this field test is also available from the authors.) We have characterized the pressure field and examined the origin of geopressures (He and Anderson, in preparation; Hart et al., 1995).

SEISMIC PREDICTION OF 4-D SEISMIC DRAINAGE EFFECTS

Laboratory measurements document the changes in acoustic reflection coefficients caused by changes in oil, gas, and water mixes, as well as effective pressure decreases. These results have been observed in the field in water and

steam floods that have produced noticeable acoustic differences over time (e.g., Nur, 1982; Dunlop et al., 1988; Breitenbach et al., 1989).

In order to quantify the seismic effects expected from the production of hydrocarbons in the LF reservoirs, we conducted a seismic amplitude modeling study by varying the acoustic properties across a hypothetical constant-thickness sandstone reservoir undergoing pressure depletion (Figure 4). Gas/oil ratio (GOR), oil/water (O/W) contact, and gas/water (G/W) changes also affect seismic amplitudes through changes in acoustic impedance across the reservoir boundaries. Tuning was avoided in this modeling study.

Differential pressure (lithostatic minus reservoir fluid) increases as hydrocarbons are drained from a reservoir, reducing seismic amplitudes in both oil and gas sands (Domenico, 1976) (Figure 4). If, however, a GOR increase occurs during production, as with the formation of a secondary gas cap, seismic amplitudes are predicted to increase, or "brighten," over time, because the acoustic effects of the fluid change dominate over the pressure depletion effects. Similarly, seismic amplitudes can dramatically decrease, or "dim out," if in addition to pressure depletion of a high GOR oil, the O/W contact migrates in a reservoir. Here, the amplitude decrease is caused by pressure depletion and is further enhanced by the drop in impedance caused by the replacement of low-velocity oil and/or gas by relatively high-velocity water.

In addition, bypassed hydrocarbons can be identified by "near-zero" changes in high seismic amplitude regions over time, if there has been little increase in differential pressure. Also, areas of sustained high seismic amplitudes can be the highest permeability drainage pathways through which hydrocarbons are moving to get to well bores. Thus, the oil, water, and gas volumes remaining in a reservoir might be derived from observing changes in seismic amplitudes over time, after carefully calibrating these observations to changes measured within wells. The question is whether time-dependent 4-D seismic monitoring can detect such changes during natural field development.

4-D SEISMIC MONITORING TECHNIQUE

Our 4-D seismic monitoring technique consists of differencing regions of high amplitudes, grown from normalized 3-D seismic surveys acquired years apart over the same field, coupled iteratively with high-resolution seismic forward and inverse modeling used to interpret acoustic changes (Anderson, et al., 1995a, patent applied for, 1995). Pattern recognition, rather than interpolation and recomputation, is used to examine similarities and differences among the seismic amplitudes of the datasets. This technique minimizes the difficulties in matching acquisition parameters, variable geometries, and technology improvements that have accompanied the development of 3-D seismic methodologies over the years.

The Pz, Tx, and Sh 3-D seismic surveys were first converted into a common coordinate grid by interpolating the surrounding bins of the Tx and Sh surveys to produce bins that correspond to the coordinate grid of the Pz survey. The preparation of the multiple 3-D seismic surveys into a 4-D dataset ready for intercomparison then requires extraction of similar power spectra from the diverse datasets. However, the normalization technique cannot completely correct for differences in reflection strength caused by orientation changes relative to rock geometry in the subsurface. Consequently, the amplitude normalizations never result in exact spectral matches (Figure 5).

Two or more 3-D seismic surveys cannot be immediately used in 4-D seismic applications because acquisition and processing parameters applied to them by different geophysical service companies often vary markedly. Consequently, the seismic attributes, such as amplitude, phase, and the frequency bandwidth of different surveys, may not be similar enough to each other even though the surveys were acquired over the same geographic location. As part of our 4-D seismic technologies software, we apply several normalization techniques to extract similar power spectra from multiple surveys. First we use spectral matching, then amplitude normalization, and finally, phase correction to minimize the differences between seismic volumes so that the processed volumes can be directly input into our region-growing and differencing analysis. As an example, consider two seismic traces observed at the same location in the 1985 and 1992 surveys (Figure 6).

To match the frequency bandwidth of the different surveys, we first compute power spectra. The frequency bandwidth common to both surveys is then uniquely identified in the frequency domain. The elimination of frequency components outside of this common frequency bandwidth is accomplished by using a zero-phase bandpass filter. This filter is then applied to both volumes, resulting in similar power spectra for the two surveys (Figure 6). Matching of the magnitudes of seismic amplitudes of the different surveys is then implemented by using histogram matching techniques on reflection strength volumes (Figure 5).

Location problems must also be dealt with. In addition to navigation errors in older surveys, discussed further below, some 3-D surveys are processed with zero-phase seafloor reflectors whereas others used minimum phase. This produces a depth mismatch between surveys, which must be corrected. We use cross-correlation techniques between individual waveforms in the various datasets to correct for this phase mismatch. Then we have to seek out the changes in spectra and phases implemented over different time windows within each survey. (A routine processing practice is to increase amplitude and decrease frequency content at depth in most seismic volumes.) We carry out numerical experiments to determine the best filters to apply to these different time windows.

The comparisons are accomplished in attribute-derivative space because we have found that only the lowest frequency amplitude spectra preserve commonality. Vertical slices that run east-west along the EI 330/338 boundary through the reflection strength volumes of each of the three surveys demonstrate the improvements in frequency content and noise abatement that have historically developed in the 3-D seismic industry (Figure 7). The Pz survey has lower frequency content than the Tx survey, and both have considerably lower signal-to-noise ratios than the Sh survey. Specifically, the waveform envelope of the reflection strength (or second reflection strength) is calculated (He and Anderson, in preparation). Figure 8 shows one such extraction from real waveforms of the Pz and Tx surveys in which the LF reflector packet is marked (Figure 8).

REGION GROWING

High-amplitude events (HAE) in any volumetric dataset are the accumulated, next-neighbor voxels of the "brightest" or most coherent energy (highest amplitudes) found within the volume. Feature-extraction operators are used to "grow" regions of HAE from seed points, which are the very highest amplitude voxels within the volume. Growth is controlled in 3-D away from the seed points by testing the

gradient in amplitudes in each direction and continuing the growth only if the gradient is below a threshold. The feature extraction methodology is robust in the sense that the final derived geometry for each volume is relatively insensitive to signal quality and ensonification parameter variations because the operation is in "gradient space."

The data fields are then segmented into volumes of similar high amplitude regions (HARs) through the use of region-growing algorithms, and data from outside these HARs are excluded from future analysis (Figure 8). It is important to note that the HARs are not bounded by "isosurfaces" connecting equal seismic amplitudes. Instead, nonlinear, region-growing operators are applied to each dataset to isolate HARs, beginning from initial "seed" points. Compare the differences between the second reflection strength and region-grown amplitude extractions (Figure 8). Rough-cut connectivity between HARs within each dataset can be obtained at this stage by properly choosing the "manifolding" operator so that low-pass spatial filtering, dilation, and erosion "grows" the connections between segmented HAR seed points.

The 4-D seismic differences between the HARs are then computed, with voxels of "near-zero" change in high amplitudes delineated as green, "brightened" amplitudes over time shown by red, and "dimouts" shown by blue (Figure 8). Edge effects are created by location errors and by the velocity differences between the different fluid mixes in this time-domain example. For example, gas cap formation significantly slows the velocities within the top of the reservoir, producing a mismatched basal edge effect on the differences between HARs (Figure 8).

The task of determining growth and shrinkage from complexly changing images is analogous to the use of nuclear magnetic resonance to quantify the growth of a cancer. The similarities and differences from one observation period to the next are used to map growth of individual HAR "tumors" (red in Figure 8), shrinkage (blue), and locations where no change in size or density has occurred (green).

THE EASTERN LF SAND

In order to test whether such theoretical seismic changes can be observed in a real reservoir, we examined the partially depleted Eastern LF oil reservoir that is located along the EI 330/338 boundary (Figure 3). The Eastern LF sand extends east-west over a 240-acre area at a depth of 6900–7000 ft (2100–2135 m) (Figure 9). A large, high-amplitude seismic anomaly (bright spot) is imaged from 1.98 to 2.06 seconds of two-way traveltime in both seismic surveys (see Figure 10). Average porosity is 27%, water saturation is 35%, and permeability is 500 md. There are proven reserves of up to 3.3 million bbl of oil in 6600 ac-ft, and probable reserves of 0.9 million bbl of oil in an additional 1800 ac-ft.

SIMILARITIES AND DIFFERENCES IN THE EASTERN LF RESERVOIR

The HARs of the Eastern LF and surrounding reservoirs were then computed. The 1985 survey is shown in green in Figure 10A and the 1988 survey in red in Figure 10B. The similarities and differences in the Eastern LF region from 1985 to 1988 were visualized, and the locations were indicated where seismic amplitudes have decreased (blue), increased (red), or remained similar (green and yellow) (Figure 10C).

Another problem with the comparison of different vintages of 3-D seismic surveys is that the navigational accuracies of the surveys have greatly improved over the last ten years. We use a cross-correlation relocation technique whereby we select an unproduced amplitude anomaly region (salt forms can also be used). That amplitude should not have changed over the time interval under consideration. An example in our study area is the IC sand, imaged in detail in the insert in Figure 10C. There was no production from this sand until after both surveys were acquired. The green and yellow areas with similar amplitudes cover 80% of the volume of the reservoir, whereas red and blue areas, indicating increases and decreases, respectively, are found around the perimeter. There are "edge effects" present that should not be there, since no production occurred. These "edge effects" are most likely caused by x-y location errors between the 3-D surveys. In order to correct for this navigation error, we use a cross-correlation technique to find the optimal fit for the IC reservoir between the two surveys. We found that the Pz survey required a two-bin shift in the inline direction and a one-bin shift in the cross-line locations. (A bin is 41 ft [12.5 m].) Such a correction is then applied to the entire datasets, resulting in an improved correlation coefficient of >90% in non-productive intervals of the two surveys (Figure 11).

Changes in amplitude over time estimate the drainage of hydrocarbons from 1985 to 1988 and identify zones of possible bypassed hydrocarbons for future drilling. Near-zero seismic differences indicate locations where there were minimal change within the HARs of the surveys, which we interpret to be possible bypassed pay (green in Figure 12A). Decreases in amplitude could be caused by water encroachment or by pressure depletion between the times of the two surveys (blue in Figure 12A), and increases in amplitude could be from GOR increases and secondary gas dissolution (red in Figure 12A).

In the eastern fault block of the Eastern LF reservoir, 105,000 bbl of oil were produced from the A-5 well over the three years between the two seismic surveys. The 4-D seismic mapping indicated that significant dimout occurred over about 220 ac-ft of the reservoir, from the east and north (blue). Production efficiencies of 480 bbl/ac-ft would be required to produce this volume from this acreage, and the efficiency from some clean sands within the EI 330 field has exceeded 800 bbl/ac-ft (Anderson et al., 1995b). Further calibration of drainage volumes versus seismic amplitude changes will require study of more extensively drained reservoirs. See the analysis of the larger and thicker (up to 120 ft [37 m]) Western LF reservoir.

VOLUMETRIC ANALYSIS OF DRAINAGE

The 4-D seismic differencing analysis produces a detailed, volumetric representation of the predicted drainage infrastructure within the bypassed pay interval, as well (yellow in Figure 12B). In fact, the 3-D pattern of bypassed hydrocarbons has surprising connectivity and logic to it. The amplitude pattern is aligned 30° to the major bounding faults. Possibly, these apparent lineations are small faults caused by a component of shear to the west accompanying extension to the south in the vicinity of the Eastern LF reservoir (thus the 30° rotation). This fault pattern, which might affect reservoir permeability, cannot be recognized in either of the primary 3-D seismic surveys but becomes a recognizable amplitude signal in the differenced, 4-D dataset.

A-8ST HORIZONTAL WELL

During the spring of 1994, well A-8ST was drilled into the Eastern LF reservoir by Texaco, as operator for the partners (Chevron, Exxon, Penzoil, Mobil, and Cochrell) (Figure 13). A 1200-ft (356-m) horizontal sidetrack was then drilled along the property line between EI 330 and 338 and the well completed. Though located before the 4-D analysis was completed, the horizontal wellpath runs along one of the yellow "no high-amplitude change" lineations imaged by the 4-D analysis. Flow rates reached a maximum of more than 1500 bbl/day of low-GOR oil during production tests in August (Figure 14). By October 1995, the well had stabilized at approximately 900 bbl/day, and cumulative production had reached more than 420,000 bbl of oil. No water has been produced to date.

SEISMIC MODEL OF DRAINAGE AT EASTERN LF TUNING THICKNESS

Quantification of the observed reservoir drainage effects is difficult for the Eastern LF reservoir because it is near the tuning thickness of the seismic sources used for the 3-D surveys. By calibrating the modeling results with the observed pressures and GORs, it was possible to compute the expected seismic amplitude changes, even at tuning thicknesses, using a 2-D finite-element forward model. First, we modeled the fluid content of a 35-ft (11-m) thick LF reservoir as 60% oil (Sw of 40%) (Figure 15A) (Sun, 1994), then we inserted a small gas cap (100% gas) in the center and drained the oil (Sw of 80%, oil saturation of 20%) to the west, replacing it with lower-pressured water, but leaving the eastern portion of the reservoir with bypassed oil (same Sw of 40%) (Figure 15B). Drainage and replacement of pressured oil with lower-pressured water produced a pronounced dimout in the predicted seismic amplitudes (blue over red) in the seismic differences plot even at tuning thickness (Figure 15C). The formation of a gas cap, even at low pressure, produced a large amplitude increase (red over blue) in the difference plot (Figure 15C). Bypassed oil remained at similar amplitudes (yellow over light blue) in the difference plot (Figure 15C).

SIMILARITIES AND DIFFERENCES IN THE WESTERN LF RESERVOIR

We then turn our attention to the Western LF reservoir, which extends along the boundary of EI 330/338 to the four corners (Figure 3). This reservoir has 3-D coverage from three surveys (Pz, Tx, Sh). Within the A fault block, the Western LF dips to the southwest from the crest of the rollover anticline in the central EI 330. It is part of a JD/KE/LF stack that is the main oil and gas producer in the field. Structural dips are on the order of 5–7 degrees, and the sand top deepens from about 6300 ft (1920 m) to over 7600 ft (2315 m) in this fault block. Figure 16 shows the locations of wells and the positions of fluid contacts, illustrating their movement with time as interpreted from the production data. Regions in red illustrate areas that have had oil replaced by gas due to expansion of a secondary gas cap updip. Regions in green are predicted to be oil-filled and are thought to have undergone no change in fluid composition. Water sweep is indicated in blue. This figure shows a large region that has been water-swept between 1972 and the present, whereas between the B-7 and B-6ST wells in the east, a secondary gas cap has grown between the time production started in 1972 and 1994 (Figure 17).

One of the interesting aspects of the oil-water contact evolution, even though derived from the sparse well coverage, is that the contact was not horizontal in 1994 but appears to cut across structural contours toward the northeast. This could indicate that the thicker sands that are located in this zone are more permeable, and fluids are being preferentially drawn from these higher-quality sands.

HORIZON AMPLITUDE EXTRACTION

We then autotracked the major amplitude reflection that corresponds to the Western LF reservoir along the structural contour of the LF in each of the surveys (Figure 18A, B, C) and extracted the variation in amplitude for each survey. These "traditional" 2-D images clearly show dimouts that are approximately parallel to structural contours (compare with Figure 16), particularly down-dip, corresponding to the oil/water contact in the southwest, and up-dip, corresponding to the shale-out to the northeast. In general, the area of high reflection decreases with time, as might be expected for a reservoir with decreasing fluid pressures and oil saturations.

Because the three datasets have been normalized, we can compute differences between surveys along this Western LF trough (Figure 18D and E). The amplitude differences, Pz–Tx, show the brightened area marking gas cap formation (red in Figure 18D) and water sweep (blue in Figure 18D) similar to those observed from the well (Figure 17), but the boundaries are more complex and less tied to structure. Depletion of the gas cap from Tx–Sh time is imaged as an amplitude dimout up-dip in Figure 18E, with brightening indicated within the newly depleted oil zone, suggesting migration down-dip of the gas cap.

The production history of the B-7 well reflects this change in the gas cap (see Figure 17). The well was put on production in 1982, and prior to 1987, the GOR remained relatively constant at about 500. However, in 1987, between the Pz and Tx survey acquisition times, the GOR increased to >20,000. In 1989, the GOR fell and the well was shut in, prior to the acquisition of the Sh survey in 1992.

VOLUMETRIC VARIATIONS OF SEISMIC DIFFERENCES

It is at this point that our 4-D seismic analysis technique departs markedly from traditional 2-D amplitude extractions on "wiggle" throughs. Region-growing within each double reflection strength dataset effectively expands the acoustic thickness of the Western LF reservoir so that volumetric variations within the HARs can be examined. We difference HARs to create volumetric representations of the seismic amplitude changes of Pz–Tx and Tx–Sh.

Because 3-D variations are difficult to convey on paper, extractions of the amplitude differences were then made into 2-D slices through the Pz–Tx and Tx–Sh HARs along planes that run parallel to the Western LF structural surface but cut through the top, middle, and bottom of the reservoir HARs. Because the differences carry memory of previous changes, we present both a fluid contact interpretation of the differences (Figure 19A) and the absolute difference image (Figure 19B). For example, a change near the B-7 well from oil at Pz time to gas at Tx time and to water at Sh time is indicated in Figure 18 first by an increase in amplitudes in the Pz–Tx difference (red), then a decrease in amplitudes in the Tx–Sh difference (blue).

The 4-D analysis indicates considerable change in the 3-D character of the fluid contacts over the time period examined. Specifically, the gas cap has indeed formed up-dip between 1985 and 1988, but has been depleted and moved

down-dip by 1992, whereas the remaining bypassed oil is predicted to be located along a thin stringer running—perhaps not coincidentally—along the property line and within the hardline among the four block boundaries. The 4-D volumetric analysis predicts that the fluid contacts do not strictly follow either structure or sand quality but are strongly influenced by their proximity to producing wells (Figure 19A).

Compare the volumetric amplitude extractions from the region-grown HARs (Figure 19A) with the planar extractions from the 2-D surfaces (Figure 18, compare with Figure 19A, B) to get some feel for the three-dimensionality of the differenced HARs. Both show the gas cap formation from Pz to Tx time, but the HAR extraction shows the down-dip migration of the high-amplitude anomaly to have migrated deeper to the south by Sh time (Figure 19A). This information is not present in the 2-D surface extraction analysis.

SUMMARY

In the future, sparsely distributed well information will be used to calibrate seismic changes observed during acoustic monitoring of entire fields, leading to reservoir characterization that can predict pressure distributions, interface changes such as O/W contact movements, porosity anomalies, permeability boundaries, GOR changes, and in particular, bypassed hydrocarbons—all in true 3-D and near real-time. However, the prediction of changes in reservoir physical parameters such as pressure and fluid content from the 4-D analysis of changes in seismic amplitudes over time is ultimately an ill-posed inverse problem. Therefore, in the future, refinements to the 4-D solution must be strongly coupled to the results of forward models of the different physical species (reservoir fluids, elastic, and acoustic).

Acknowledgments

An accompanying CD-ROM containing detailed accounts of this and related field studies of the Eugene Island 330 field is available for shipping and handling fees of $10 from David Roach, GBRN, Lamont-Doherty Earth Observatory, Palisades, NY 10964 (Internet address roach@ldeo.columbia.edu, phone 914-365-8330, fax 914-359-1631). We wish to thank the corporate affiliates of the GBRN for supporting this work: Amoco, Arco, BP, Chevron, Conoco, Elf, Exxon, Mobil, Pennzoil, Shell, Texaco, and Unocal. The work was cost-shared through DOE contract # DE-FC22-93BC14961.

REFERENCES CITED

Alexander, L., and P. B. Flemings, 1995, Geologic evolution of a Plio-Pleistocene salt withdrawal mini-basin: Block 330, Eugene Island, South Addition, Offshore Louisiana: AAPG Bulletin, v. 79 n. 12, p. 1737–1756.

Anderson, R. N., and W. He, 1995, 4-D seismic interpretation techniques for the detection of drainage and migration in oil and gas reservoirs: U.S. Letters patent applied for.

Anderson, R. N., A. Boulanger, W. He, Y. F. Sun, L. Xu, 1995a, 4-D seismic imaging of drainage and pressure compartmentalization in the Gulf of Mexico: Oil and Gas Journal. Part 1, March 28; Part 2, April 4.

Anderson, R. N., P. B. Flemings, and S. Losh, 1995b, The GBRN/DOE Eugene Island Dynamic Enhanced Recovery Project: CD-ROM, Lamont Press.

Breitenbach, E. A., G. A. King, and K. N. B. Dunlop, 1989, The range of applications of reservoir monitoring: SPE Paper 19853.

Domenico, S. N., 1976, Effect of brine–gas mixture on velocity in an unconsolidated sand reservoir: Geophysics, v. 41, p. 882–894.

Dunlop, K. N. B., G.A. King, and E. A. Breitenbach, 1988, Monitoring of oil/water fronts by direct measurement; SPE Paper 18271.

Hart, B. S., P. B. Flemings, and A. Deshpande, 1995, Porosity and pressure: role of compaction disequilibrium in the development of geopressures in a Gulf Coast Pleistocene basin: Geology, v. 23, p. 45–48.

Hart, B. S., P. B. Flemings, D. M. Sibley, and B. Bishop, 1996, Facies Architecture of a shelf margin lowstand complex, Eugene Island Block 330 Field, Louisiana Offshore: AAPG Studies in Geology No. 42/SEG Geophysical Development Series No. 5, AAPG/SEG, Tulsa.

Holland, D. S., J. B. Leedy, and D. R. Lammlein, 1990, Eugene Island Block 330 Field-U.S.A. Offshore Louisiana, in E. A. Beaumont and N. H. Foster, compilers, Structural Traps III: Tectonic Fold and Fault Traps: Treatise of Petroleum Geology, Atlas of Oil and Gas Fields, AAPG, Tulsa, p. 103–143.

Nur, A. M., 1982, Seismic imaging in enhanced recovery; SPE Paper 10680.

Sun, Y. F., 1994, On the foundations of the dynamical theory of fractured porous media and the gravity variations caused by dilatancy, Ph.D. dissertation, Columbia University.

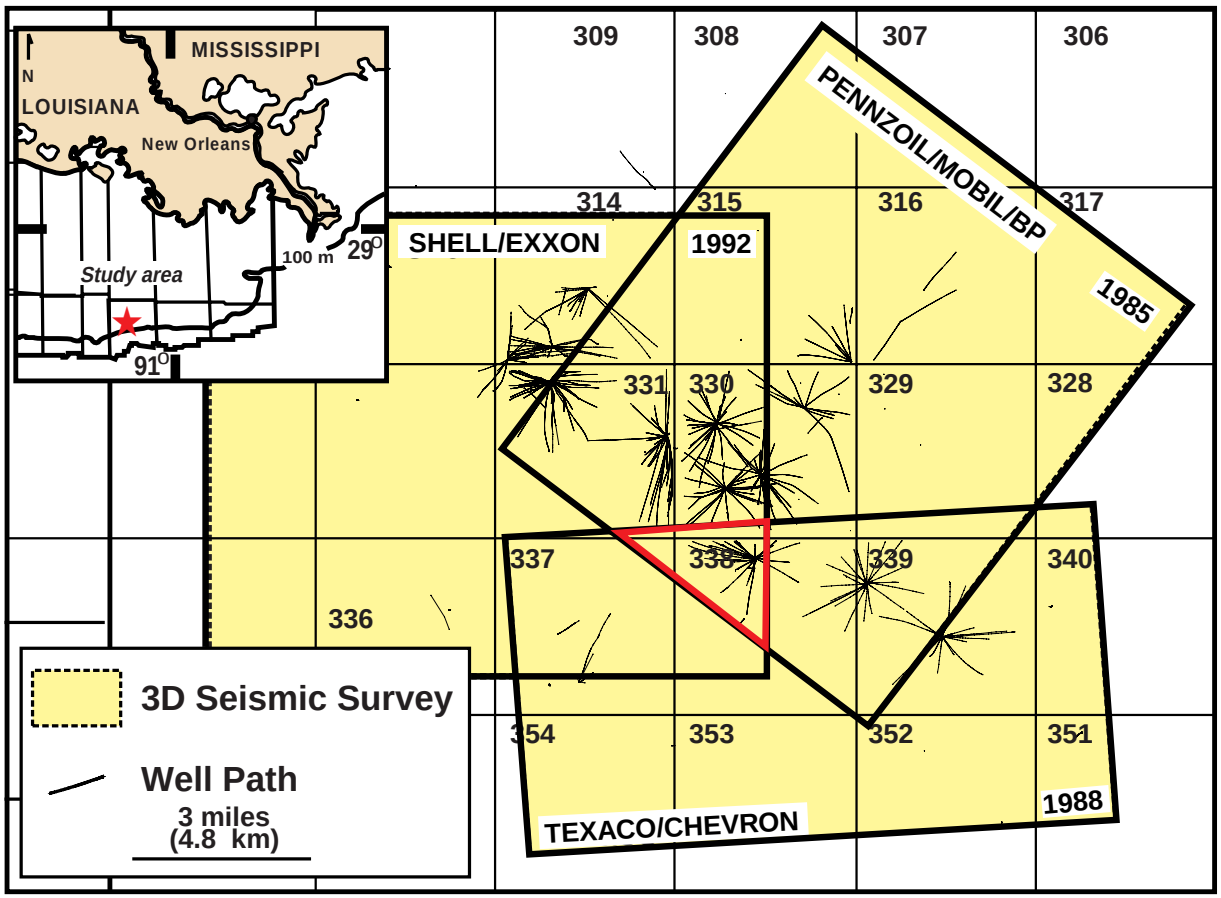

FIGURE 1. Location map of overlapping 3-D surveys. Red triangle is study area.

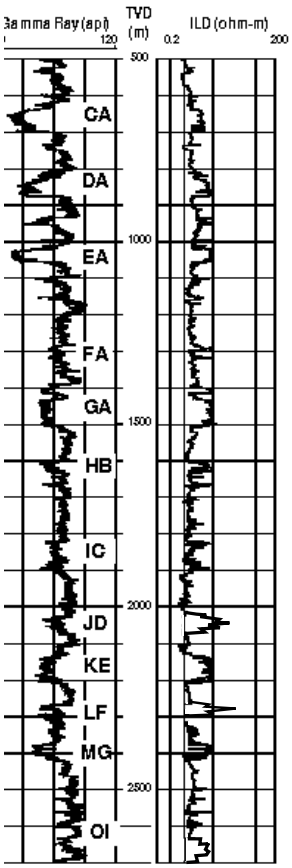

FIGURE 2. El 330 type log, from Holland et al., 1990.

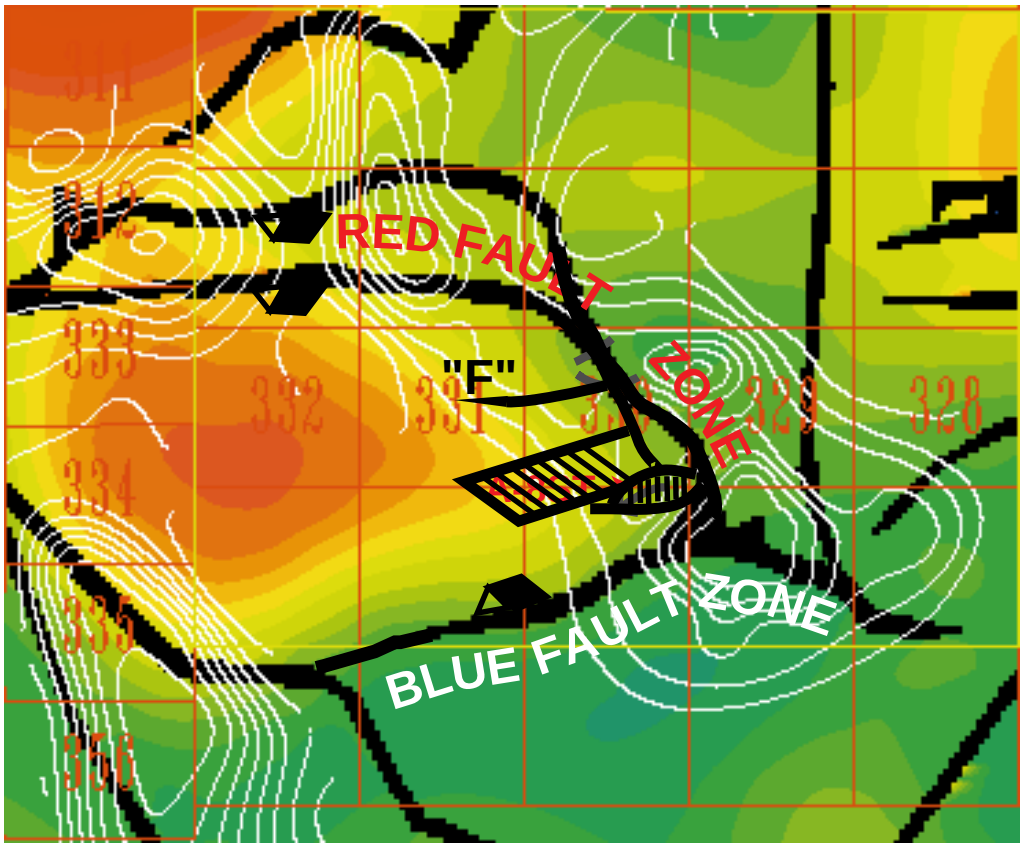

FIGURE 3. The Eugene Island 330 minibasin, shown by depth to the top-of-geopressure surface. Hot colors are deep; red = 15,000 ft. Green colors are shallow (darkest green = 5000 ft). Contour interval = 1000 ft (He and Anderson, in preparation). White contours are top-of-salt (top contour = 10,000 ft; interval = 2000 ft), and black lines are faults. Vertical bars are "Eastern LF," and diagonal bars show the distribution of the "Western LF" reservoirs.

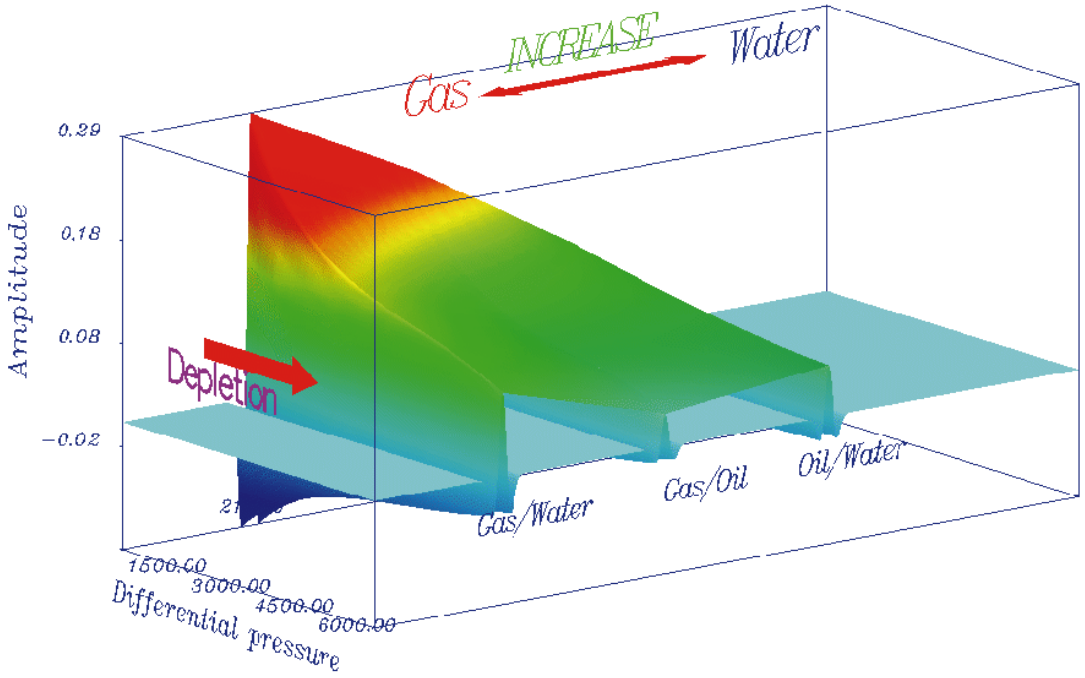

FIGURE 4. Model study of effects of fluid change on reflectivity in the EL 330 sands. A waveform modeling study was carried out to map the changes in seismic amplitude caused by the variation in oil/gas/water and formation pressure during depletion of a reservoir. The study is tracking the wavelet change across the upper interface of a thick sand with various fluid contrasts across the boundary.

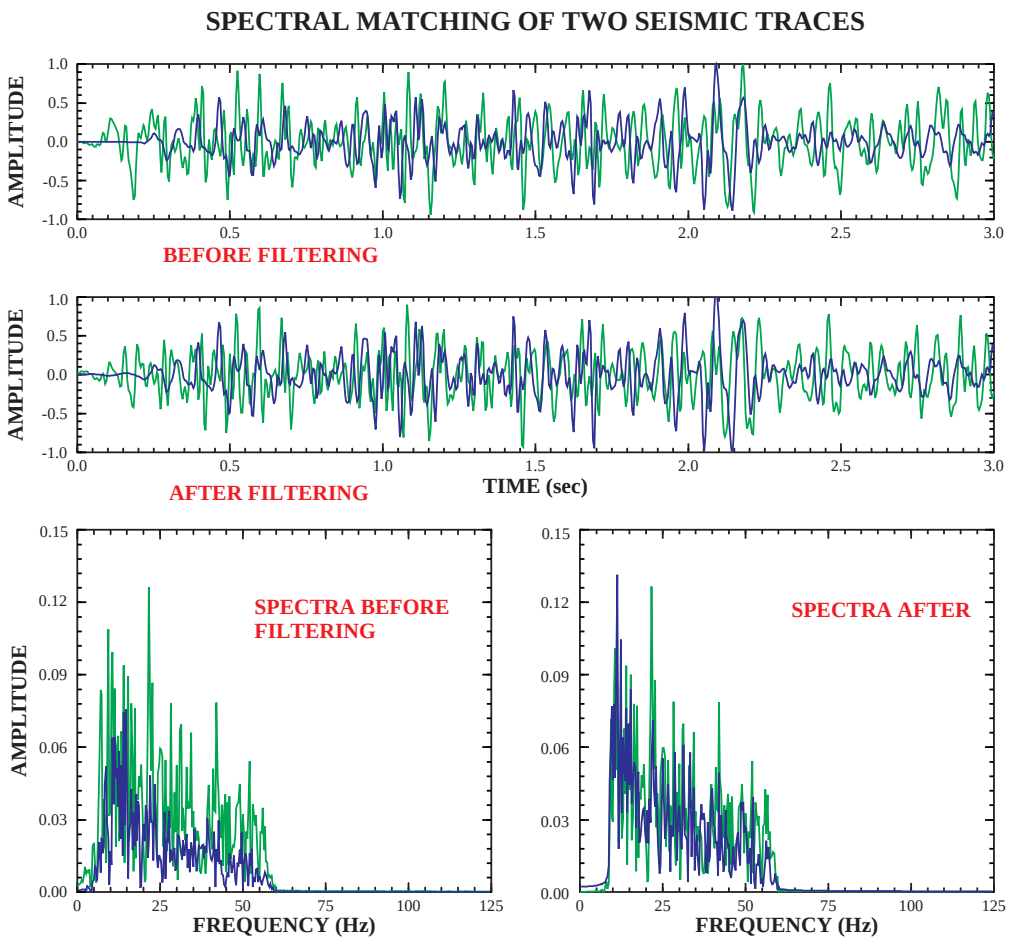

FIGURE 5. Spectral matching of two seismic traces.

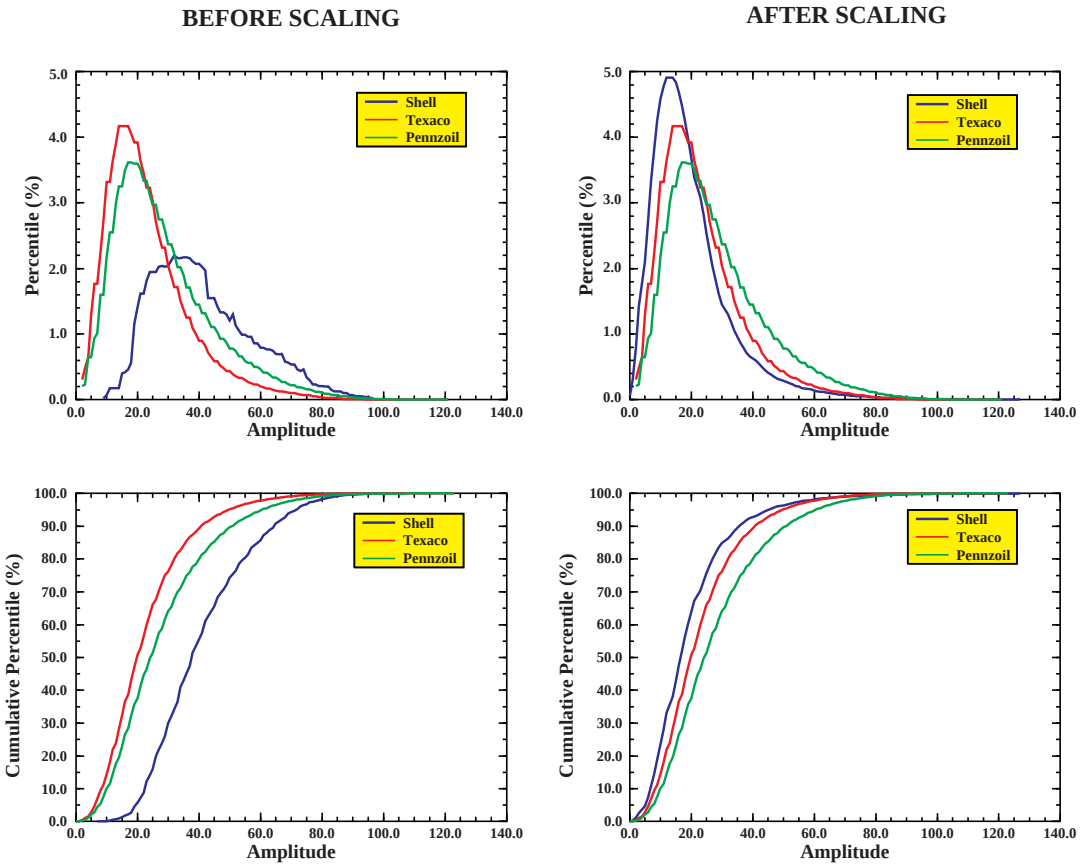

FIGURE 6. Spectral matching in 3-D seismic datasets. Histograms of amplitude content of reflection strength datasets before (left) and after (right) normalization.

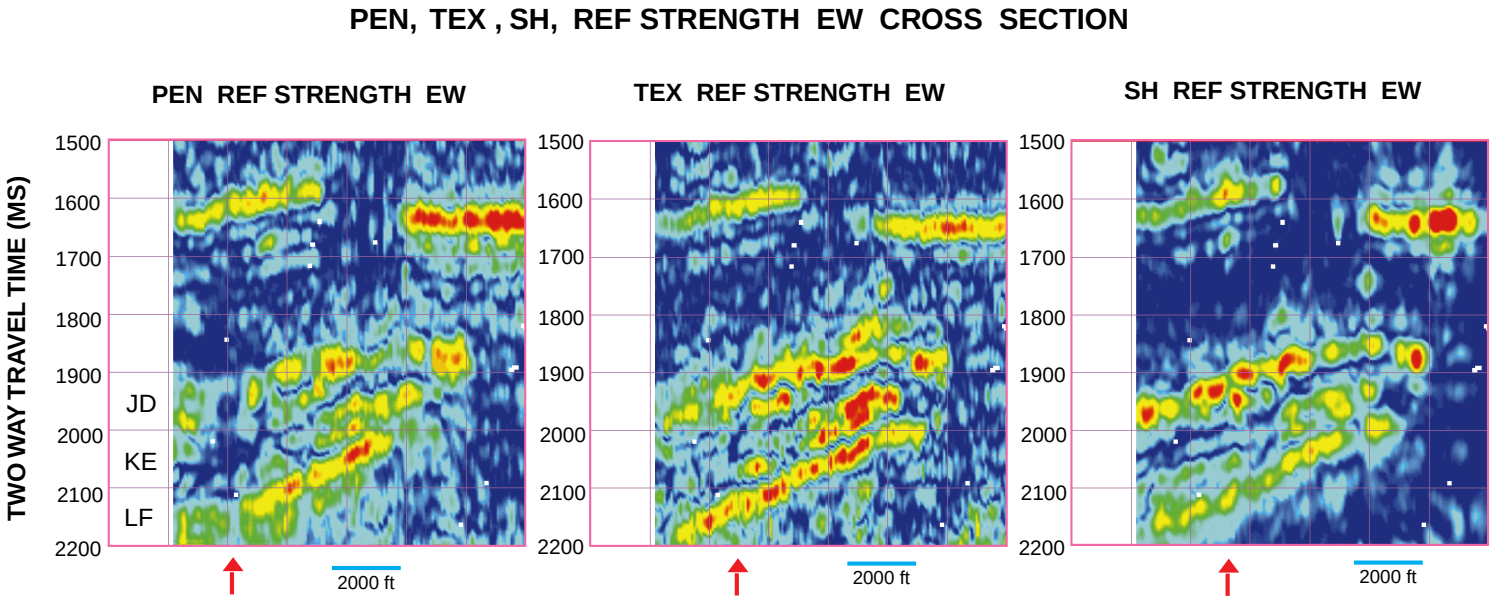

FIGURE 7. Seismic profile along the EI 330/338 property line. Amplitude attribute images of three surveys running along the boundary of EI blocks 330 and 338. Arrow is 4 corners.

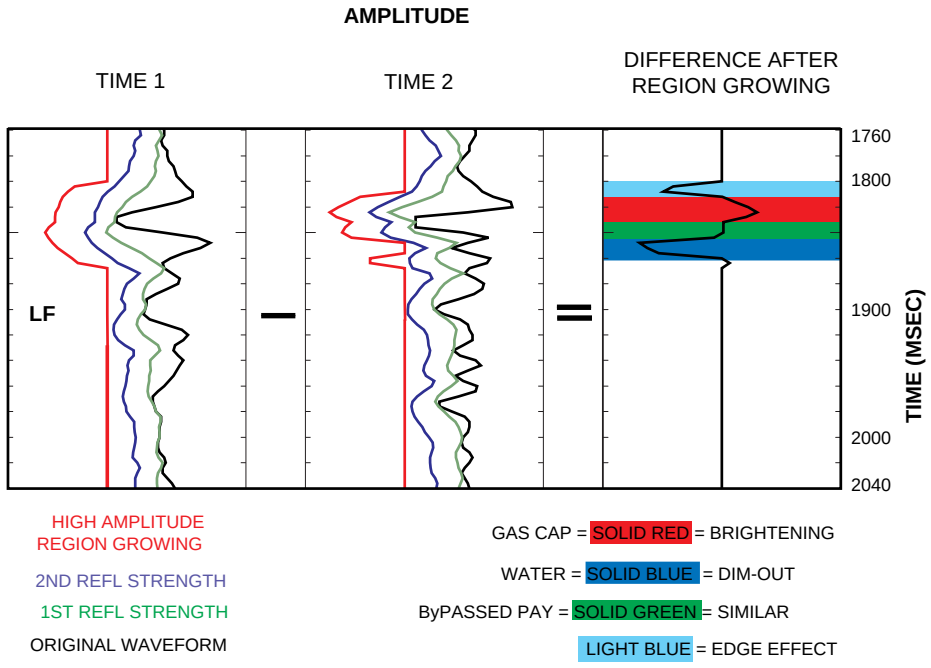

FIGURE 8. 4-D seismic differencing technique; example of growth of a high-amplitude region.

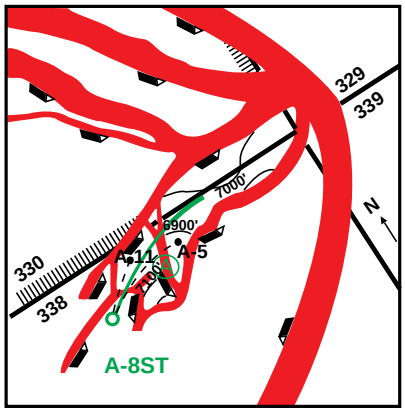

FIGURE 9. Location of Eastern LF reservoir. Structure of Eastern LF sand is indicated by contour. A-8ST is indicated in green. "A" fault is not distinct in the seismic data, but is clear in the 4-D seismic differences.

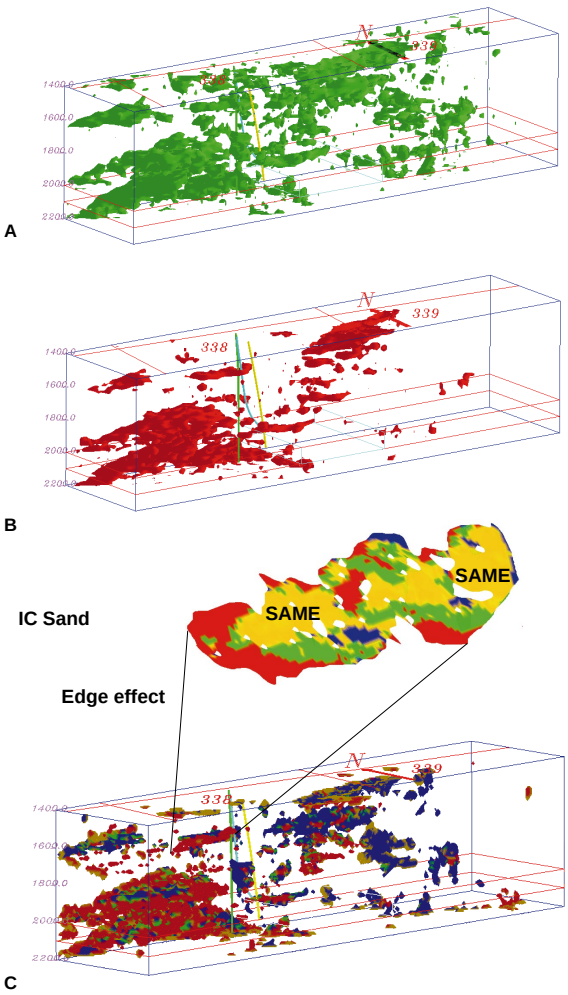

FIGURE 10. Seismic amplitude along the EI 330/338 boundary. (A) Amplitude envelopes around high seismic amplitudes from 1.4 to 2.2 seconds of traveltime for the Pennzoil (1985) survey, shown in green. The small box indicates the LF sand. (B) Texaco (1988) survey, shown in red. (C) The differences between Figure 10A and 10B in seismic amplitudes within the high-amplitude surfaces with dimouts from 1985 to 1988 indicated in blue and amplitude similarities shown in gold and green. Brightening is red.

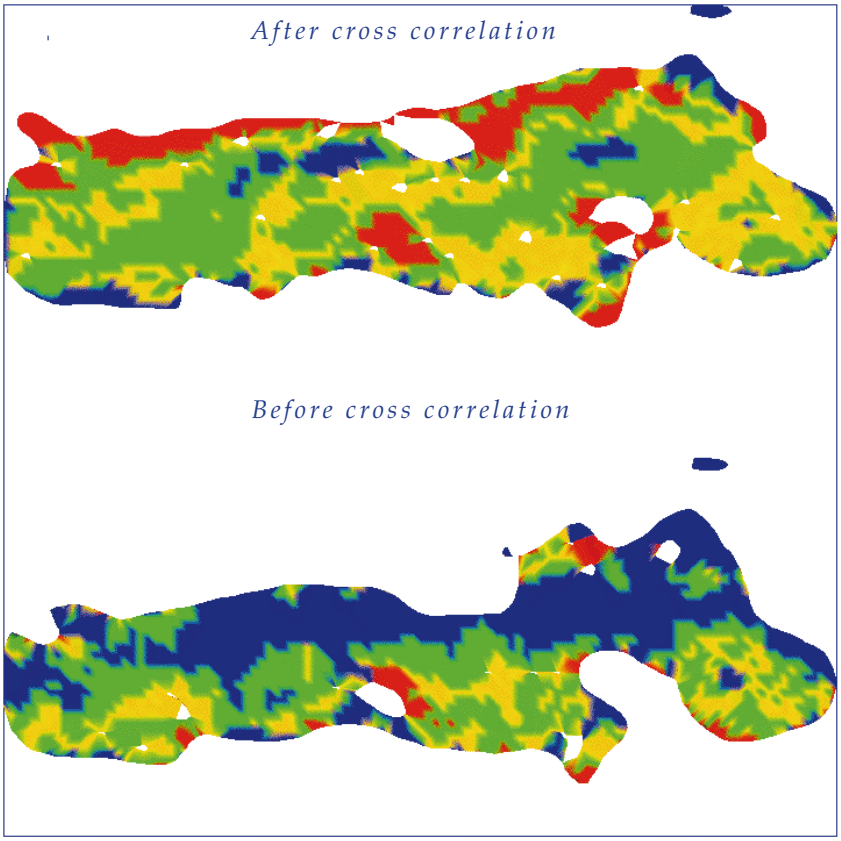

FIGURE 11. IC sand reservoir (preproduction). Cross correlation is used to correct navigation errors in older surveys. The fit between the two surveys has been improved from 80% (bottom) to 90% (top) in the IC reservoir. The amplitude differences between the two surveys are ≤5% (yellow), ≤10% (green), >10% old-new (blue) and >10% new-old (red).

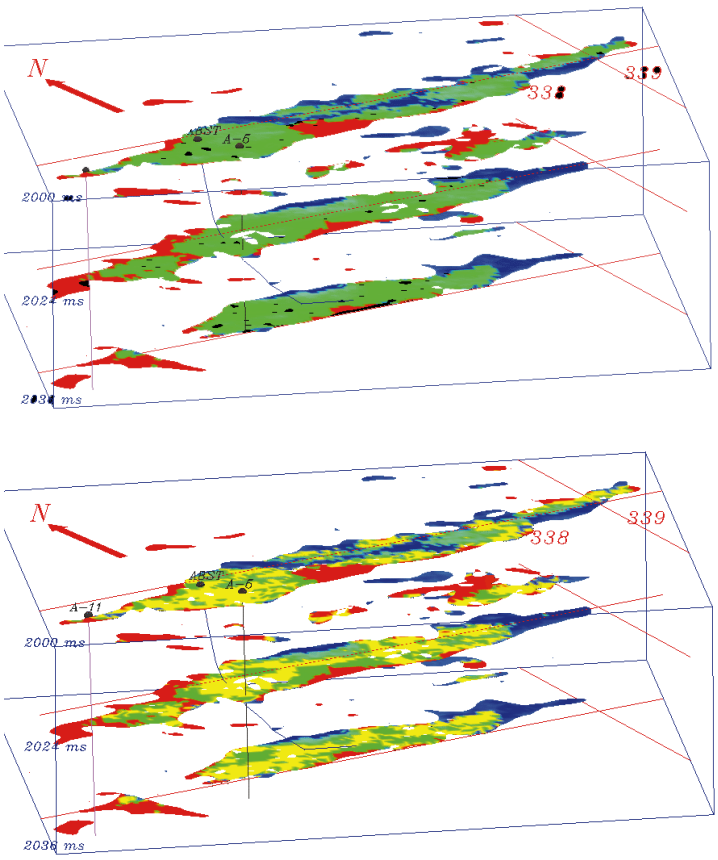

FIGURE 12. Eastern LF seismic amplitude differences. (A) Green = no change in high amplitudes, the most prospective region; blue = dimout from production; red = amplitude increase caused by gas/oil ratio increase with production. (B) Yellow = the region within the HAE with no measurable change (<10%) in seismic amplitude from 1985 to 1988. Green = the region that still has high amplitudes, but within which some change (10–30%) has been detected.

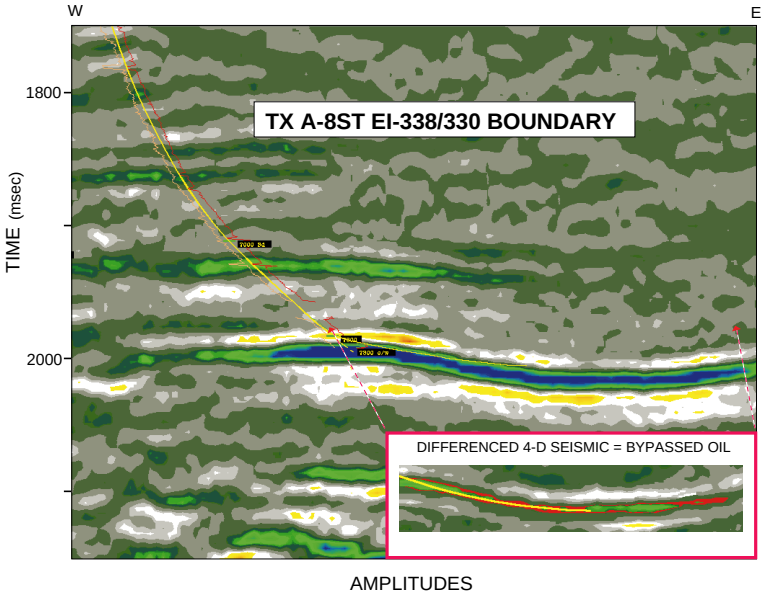

FIGURE 13. Horizontal well into Eastern LF reservoir in 1994. West-east seismic profile through the property boundary of EI 330/338, showing Eastern LF sand reservoir and blowup of the similarities and differences between seismic amplitudes from 1985 to 1988. The A-8ST horizontal well (yellow) targeted bypassed pay (red).

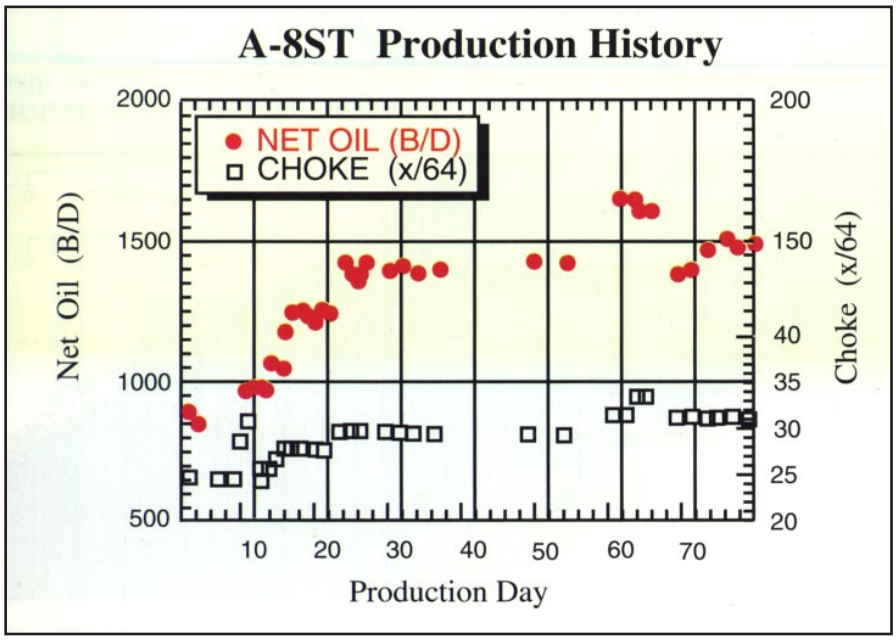

FIGURE 14. The production history of the A-8ST horizontal well for the first 80 days of production. More than a year into production, the well was producing about 1000 bbl/d.

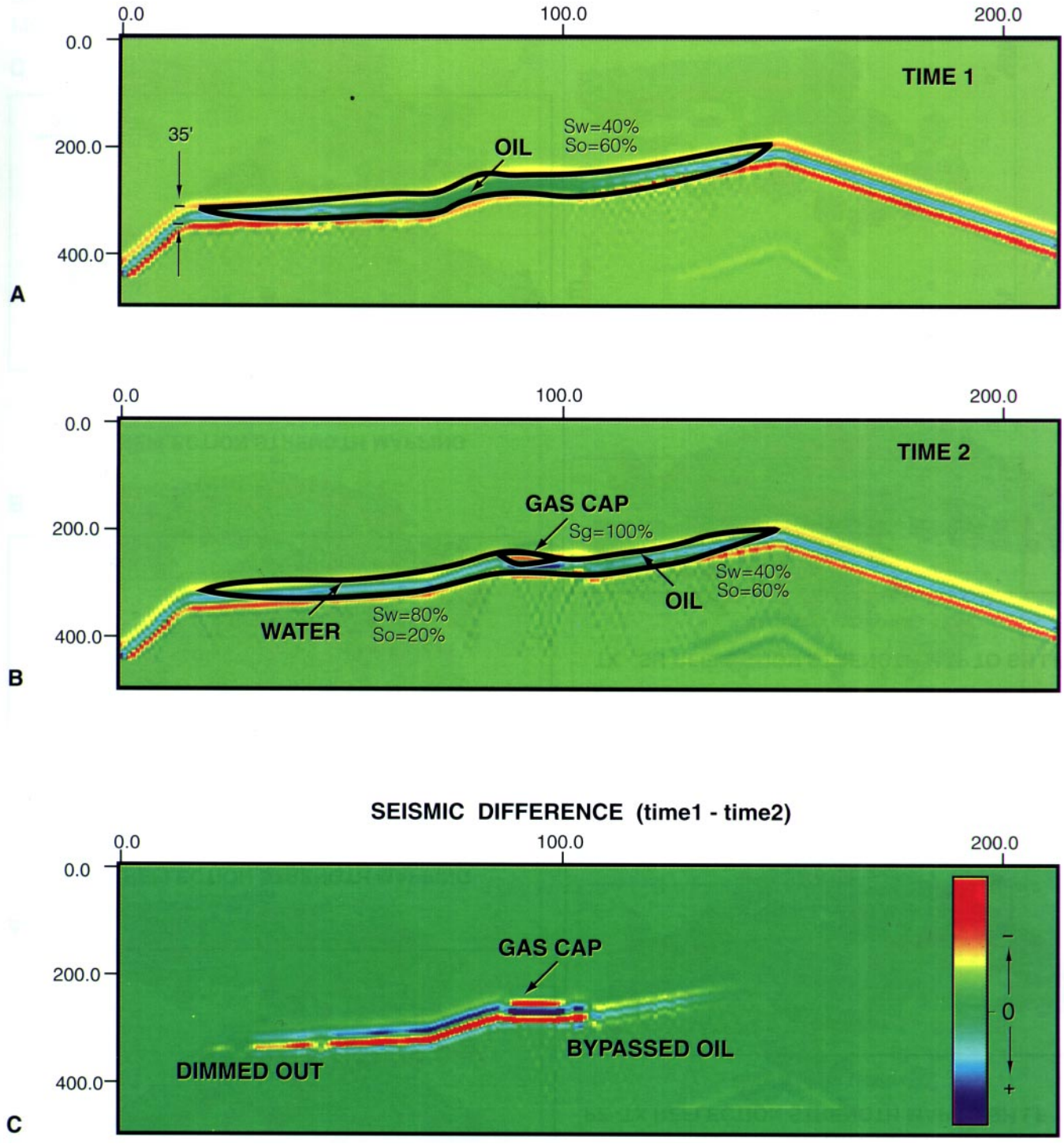

FIGURE 15. LF reservoir forward model. Seismic model of eastern LF reservoir, with oil/gas/water and pressure changes that were observed between 1985 (Time 1) and 1988 (Time 2), as indicated by production logs and pressure monitoring. Dimouts are predicted where the S_w has increased, and brightening where the central gas cap formed.

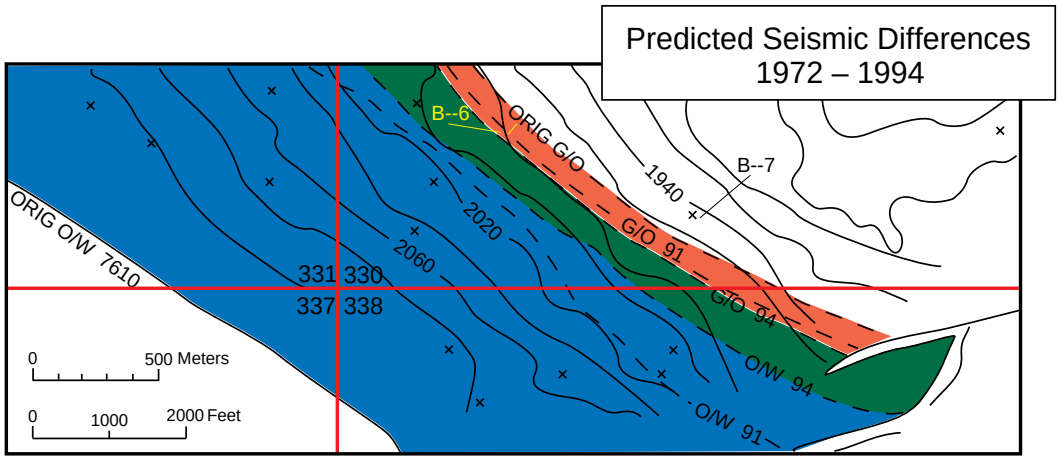

FIGURE 16. Map showing interpreted changes in fluid composition based on production data from wells only (locations indicated by x's). Compare this with observed seismic changes in Figure 18.

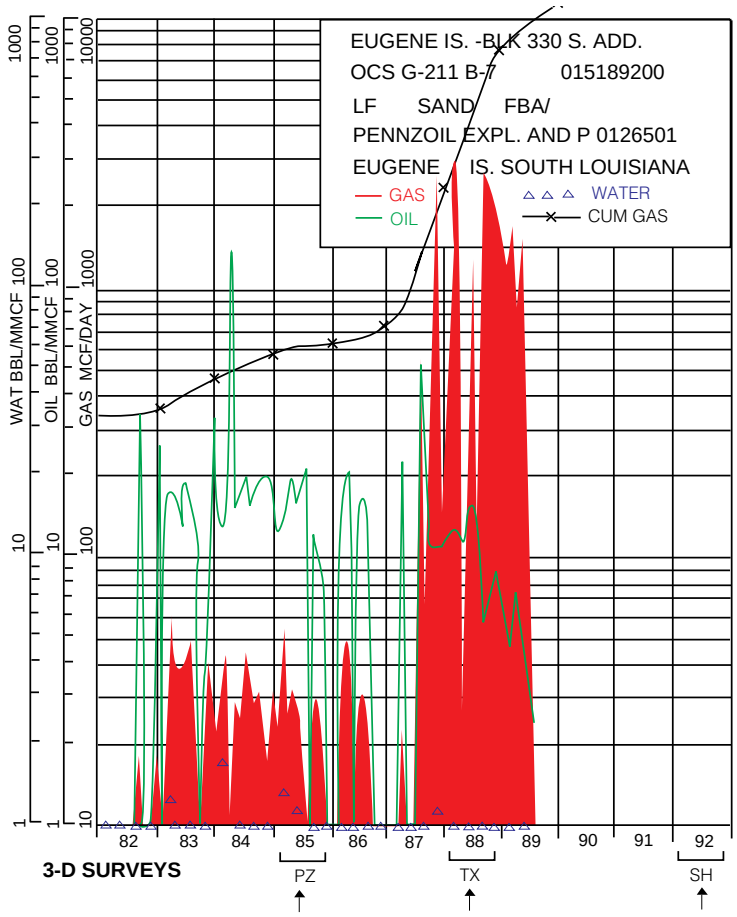

FIGURE 17. Production history of the B-7 well showing the increase in gas production between the Pz and Tx seismic surveys, then the watering-out of the well before the Sh survey.

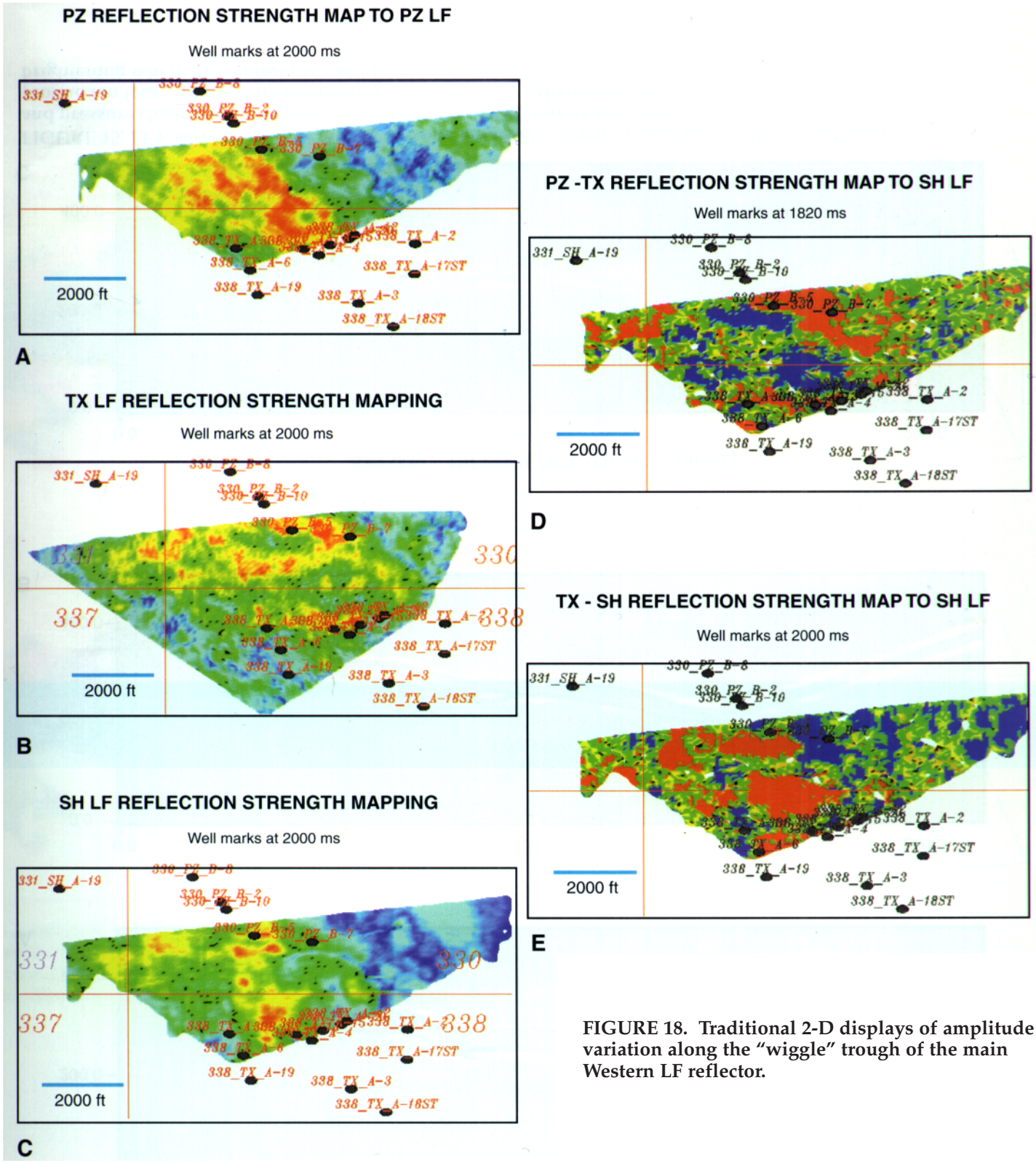

FIGURE 18. Traditional 2-D displays of amplitude variation along the "wiggle" trough of the main Western LF reflector.

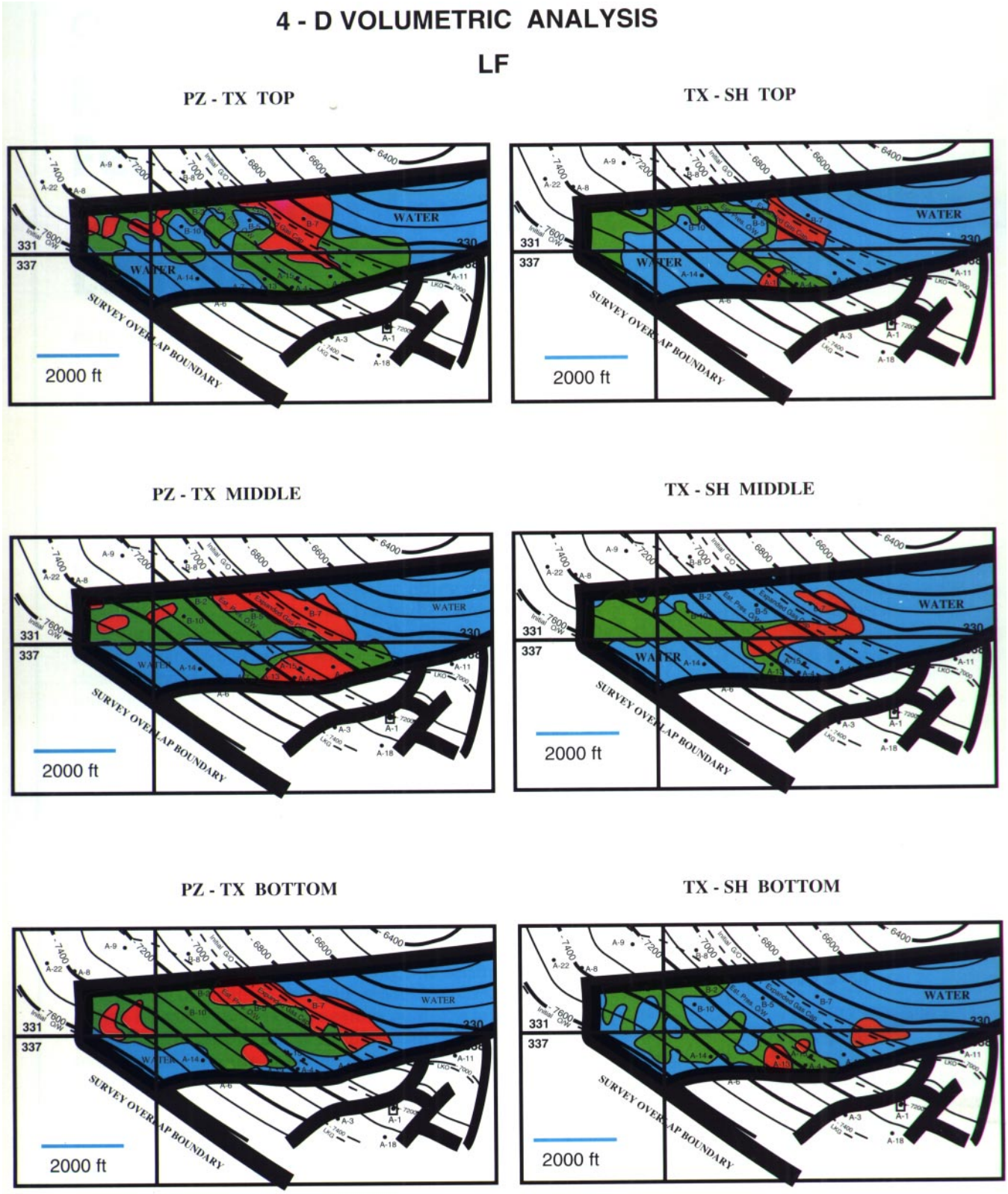

FIGURE 19A. Fluid contact interpretation of drainage in the Western LF reservoir. Blue is water, red is gas, and green is predicted location of bypassed oil.

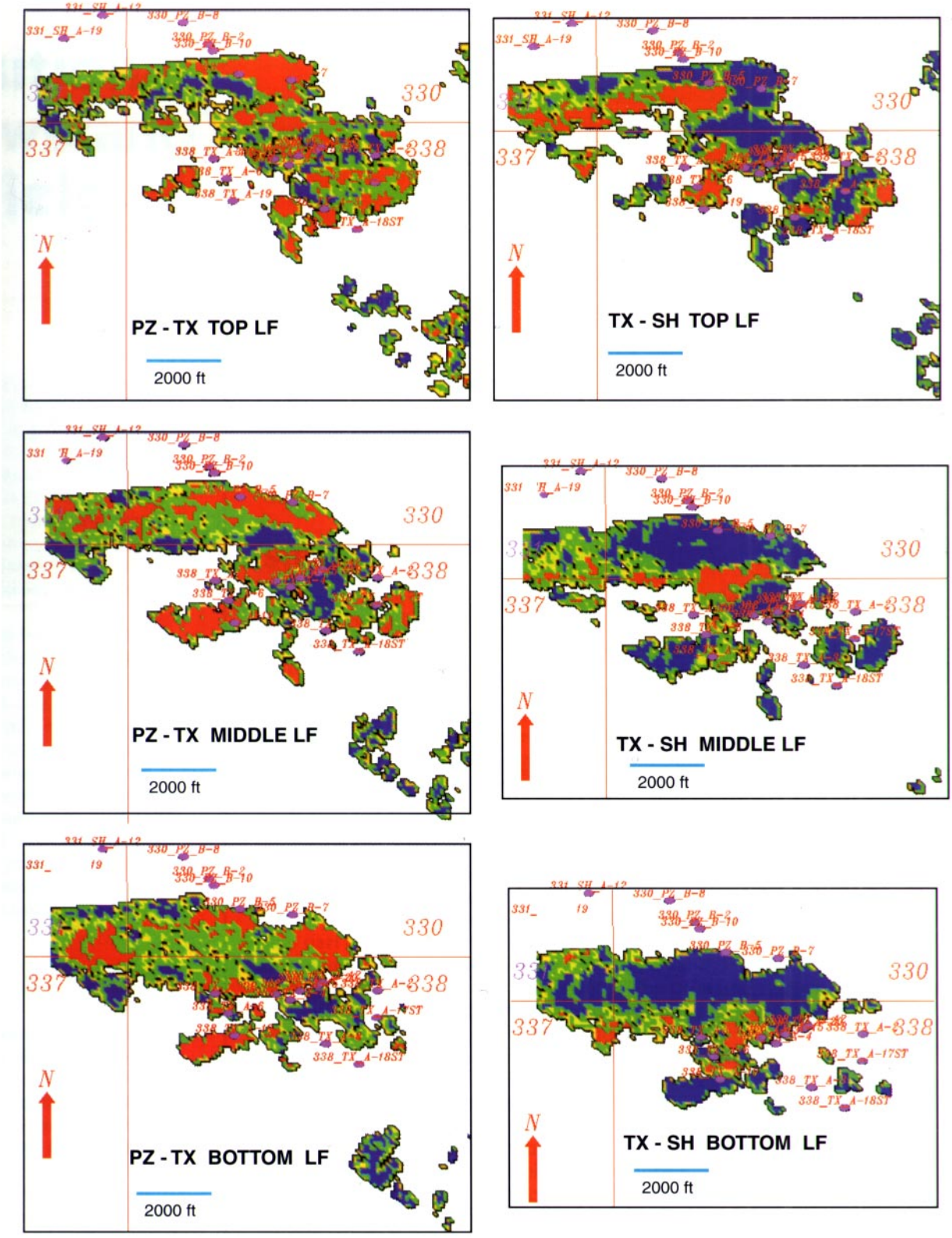

FIGURE 19B. Difference images of Western LF reservoir used to determine oil/gas/water boundaries in Figure 19A.